# In-situ characterization of walls' thermal resistance
## An extension to the ISO 9869 standard method

Rasooli, Arash; Itard, Laure

**DOI**
10.1016/j.enbuild.2018.09.004

**Publication date**
2018

**Document Version**
Final published version

**Published in**
Energy and Buildings

**Citation (APA)**
Rasooli, A., & Itard, L. (2018). In-situ characterization of walls' thermal resistance: An extension to the ISO 9869 standard method. *Energy and Buildings*, *179*, 374-383. https://doi.org/10.1016/j.enbuild.2018.09.004

Energy & Buildings 179 (2018) 374–383

Contents lists available at ScienceDirect

Energy & Buildings

journal homepage: www.elsevier.com/locate/enbuild

# In-situ characterization of walls' thermal resistance: An extension to the ISO 9869 standard method

Arash Rasooli[a,*], Laure Itard[a]

[a] Delft University of Technology, Faculty of Architecture and the Built Environment, OTB: Research for the Built Environment, Julianalaan 134, 2628 BL Delft, The Netherlands

ARTICLE INFO

*Article history:*
Received 8 May 2018
Revised 20 July 2018
Accepted 1 September 2018
Available online 22 September 2018

*Keywords:*
Thermal resistance
In-situ measurement
ISO 9869 standard
Heat transfer simulation
Heat flux sensor

ABSTRACT

Accurate and reliable in-situ characterization of buildings' thermal envelope is of high significance to determine actual energy use and thermal comfort. In this context, walls' thermal resistance is one of the most critical properties to be identified. Regardless the numerous studies being carried out to accurately measure the actual thermal resistance of walls on site, the heat flow meter method suggested by the ISO 9869 standard is the one being applied the most. The method requires one heat flux sensor and two thermocouples to measure and estimate the average thermal resistance over a sufficiently long period. Despite the advantages of this method, two problems have been seen in practice: long duration and precision problem. The present article describes and demonstrates how modifications to this standard method can improve the results of the in-situ measurements in terms of duration and precision. Simulations and experiments have been applied to show the effect of using an additional heat flux sensor, opposite to the first one. The modified method aids in obtaining the thermal resistance with a higher precision in a shorter period of time.



## 1. Introduction

Buildings are known to be responsible for a considerable share of worldwide energy consumption [1]. Apart from the occupant behavior, a building's individual energy consumption is highly dependent on the thermo-physical characteristics of its envelope [2,3]. One of the most critical characteristics is the walls' thermal resistance $R_c$-value, whose accuracy of determination can significantly influence the accuracy of buildings' total energy consumption prediction [4,5]. The accuracy of these predictions is critical in the sense that they are generally used as the basis for the majority of decisions and policies [6]. Therefore, accurate estimation of the actual $R_c$-value of the wall sections is known to be of high importance. Numerous experimental and computational studies [7,8] have aimed at accurate determination of this parameter using in-lab/in-situ and static (steady state)/dynamic (transient) approaches. On one hand, calculation of the $R_c$-value can be quite simply done according to ISO 6946 [9], in which the computation methods for thermal resistance estimation based on the construction of the samples are provided. The exact construction of the existing walls is generally unknown and thus, in such cases, this calculation method is not appropriate. On the other hand, many studies have shown the difference between the thermo-physical characteristics calculated or claimed as the design values and the ones measured experimentally during measurement campaigns [10–15], implying the necessity of performing measurements and the investigation of these measurements for being accurate enough. Regardless the numerous studies being carried out to accurately measure the actual thermal resistance of walls on site, the heat flow meter method suggested by the ISO 9869 [16] and ASTM 1046 and 1155 [17,18] standards, which are very similar, are the ones being applied the most. Despite the advantages of these methods, two problems have been seen in practice: long duration and precision problem. The present article describes and demonstrates how modifications to ISO 9869 can improve the results of the in-situ measurements in terms of duration and precision.

## 2. State-of-the-art

Various measurement techniques have been developed including steady state and transient methods applied in-situ [19,20] and in-lab [21–27] to estimate the accurate thermal resistance, with and without relying on steady state (and quasi-steady state) as-

* Corresponding author.
*E-mail addresses:* A.Rasooli@tudelft.nl (A. Rasooli), L.C.M.Itard@tudelft.nl (L. Itard).

https://doi.org/10.1016/j.enbuild.2018.09.004

**Nomenclature**

*Symbols*

| | |
|---|---|
| $C$ | Specific heat capacity (J kg$^{-1}$ K$^{-1}$) |
| $k$ | Thermal conductivity (W m$^{-1}$ K$^{-1}$) |
| $l$ | Wall thickness (m) |
| $m$ | Minimum required measurement period (h) |
| $\dot{q}$ | Heat flux (W m$^{-2}$) |
| $R_c$ | Conductive thermal resistance (m$^2$ K W$^{-1}$) |
| $T$ | Temperature (K) |

*Superscripts*

| | |
|---|---|
| $\infty$ | Fluid medium (air) |
| $t$ | Time (h) |
| $th$ | Theoretical value |

*Greek letters*

| | |
|---|---|
| $\alpha$ | Convective heat transfer coefficient (W m$^{-2}$ K$^{-1}$) |
| $\Delta$ | Difference |
| $\rho$ | Density (kg m$^{-3}$) |

*Indices*

| | |
|---|---|
| *acc* | Accumulation of heat |
| *ave* | Average |
| *in* | Associated with the interior surface |
| *out* | Associated with the exterior surface |
| 1 | Associated with the interior surface |
| 2 | Associated with the exterior surface |

*Abbreviation*

| | |
|---|---|
| HFS | Heat flux sensor |

sumption. The steady state and the quasi-steady state assumptions, which are the basis of $R_c$-value measurements, tend to become problematic when the temperature and heat flux fluctuations are extreme (e.g. unsteady climatic conditions). Therefore, in case of static-based methods, usually additional modifications such as on-site data corrections for large temperature drifts [28] and including the wind velocity effects [29] are addressed to improve the measurement accuracy. Other advanced transient data analysis methods such as regression modelling and ARX-modelling have been used to improve the reliability and robustness of the results [30]. In the recent past, applying the measurement data to mathematical models has become more popular. This type of methodology includes stochastic grey box modelling and inverse modelling [31,32]. For instance, lumped thermal mass models and Bayesian statistical analysis of temperature and heat flux measurements, have been applied to estimate reliable thermo-physical properties of walls [33].

In summary, there is a large variety of scientific theoretical and practical methods available to determine the $R_c$-value of existing walls. However, if such determination is to be carried out in large scale (e.g. nationwide monitoring campaigns), a common trusted procedure is needed to be followed as a reference. For this purpose, standards have been developed and applied widely [11, 12,34] to characterize the walls' thermal resistance via in-situ measurements. The standard practices for in-situ evaluation of wall's thermal resistance include the international standard ISO 9869 [16] and the American standard ASTM 1046 and 1155 [17,18]. Beside small differences in details, the principles of the two standards are the same. In 2017, these two methods have been compared [35] in detailed in different case studies finding out the time requirements, measurement conditions, and constraints to improve the results. In these methods, the thermal resistance of a wall is measured using two thermocouples mounted opposite to each other on two sides of the wall and a heat flux sensor (HFS) mounted next to the thermocouple on one side, preferably the interior side because of higher stability in temperature. For accurate post processing of the data, information about the construction is required to include the effect of heat storage and dynamic heat accumulation. In case of unknown construction, if a non-destructive inspection is to be carried out, such information is not available [36] and therefore, corrections cannot take place. This is known to significantly influence the accuracy, leading to a less reliable result. According to the studies in which the method has been applied, there are two main problems which the method can be associated with: First, the long duration of the measurements due to unstable boundary conditions [11,16] and second, the problem of $R_c$-value precision. The duration required for the $R_c$-value to be reported, fulfilling the criteria of ISO 9869 [16], can be very long. This becomes a barrier and therefore, makes it difficult for the method to be applied often in practice. The results of the ISO 9869 [16] Average Method are highly dependent on the temperature and heat flux circumstances. The profile of heat flux and temperature determine the final value and the time required for the convergence to occur. According to ISO 9869 [16], presuming that all conditions are taken into account, in order to report an acceptable $R_c$-value, the main criteria to fulfill and stop the measurement include the following:

1. The measurement period should take at least 72 h with a specific range of sampling and logging intervals.
2. The $R_c$-value obtained from the last two measurement day should not differ by more than 5%.
3. The difference between $R_c$-values obtained from the first and last certain number of days [16] is within 5%.

Other criteria such as heat content and dynamic data processing [37] are generally not applicable in in-situ measurements as the exact construction is unknown. The cumulative $R_c$-value is reported for each day (including the average of the previous days). As this process continues, the curve of the reported $R_c$-values converges to a certain value, which is the average of the whole measuring period, fulfilling the aforementioned conditions.

Practical experiments, however, in which a second heat flux was installed [19] on the opposite side of the one recommended by ISO 9869 have shown that the two $R_c$-values are measured based on two heat fluxes (indoor and outdoor wall surface), could converge to two different final values (not in the same range), both fulfilling the criteria of ISO 9869. As seen also in other studies [11,19], it may happen that if the test continues, the final convergence value starts moving towards another convergence point, or that the two $R_c$-values do not converge to the same value even after a relatively long period. This poses a question about which of the values to report as the actual $R_c$-value, and if it would not be better to report the average of the two values.

According to the ISO 9868 [16] Average Method, the $R_c$-value of a wall, based on measurements of $\Delta T$ (the surface temperature gradient), $\dot{q}$ (the heat flux), and $t$ (the time interval), can be derived as follows:

$$R_c = \sum_{t=0}^{m} \Delta T^t / \sum_{t=0}^{m} \dot{q}^t \tag{1}$$

According to (1), the instantaneous $R_c$-value at each side is different because the two instantaneous heat fluxes $\dot{q}^t$ at both sides of the wall vary, thanks to the thermal mass (resulting in $\dot{q}_{acc}$ in Fig. 1), and temperature and heat flux fluctuations on two sides of the wall. However, in long term, based on energy conservation, the summation of $(\dot{q}^t)_1$ and $(\dot{q}^t)_2$ are equal. According to ISO 9869 [16], such summation is to be done in a long enough time period (at least 72 h for light elements and more than a week for heavy

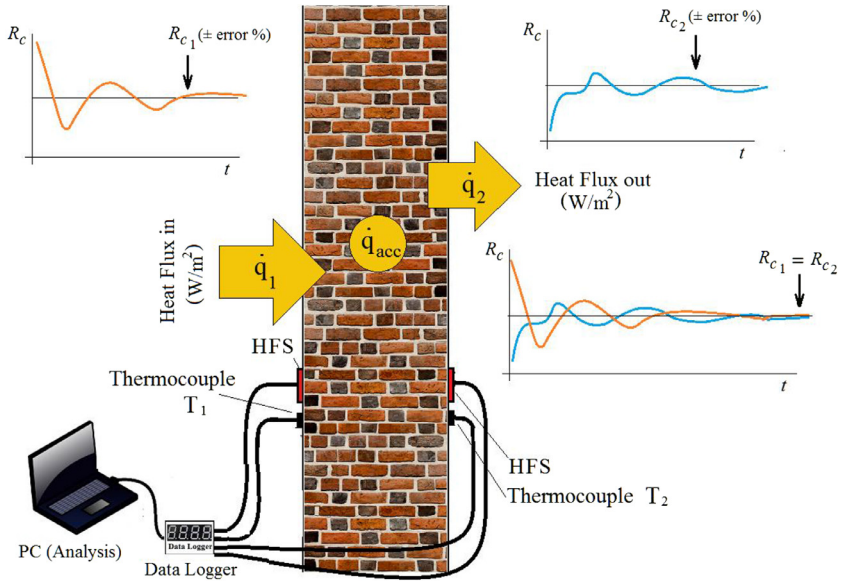


**Fig. 1.** General configuration of ISO 9869 standard measurement with one extra HFS added. The two $R_c$-values based on each HFS differ and in short term converge to different values.

elements [16]). In this case:

$$\sum_{t=0}^{m}\left(\dot{q}^t\right)_1 = \sum_{t=0}^{m}\left(\dot{q}^t\right)_2 \tag{2}$$

The validity of (2) depends highly on the construction, time period, and the boundary conditions (climatic conditions). In short term, by measuring the heat flux on either side of the wall, one may find a different $R_c$-value than by measuring the heat flux on the opposite side. The two $R_c$-values are expected to converge to the same final value over a long-enough periods (see Fig. 1):

$$R_{c\,1} = \sum_{t=0}^{m}\Delta T^t / \sum_{t=0}^{m}\left(\dot{q}^t\right)_1 = R_{c\,2} = \sum_{t=0}^{m}\Delta T^t / \sum_{t=0}^{m}\left(\dot{q}^t\right)_2 \tag{3}$$

where $R_{c1}$ and $R_{c2}$ are the $R_c$-values obtained based on cumulative heat flux at the interior and exterior surface, respectively.

The main aim of this study is to address the two aforementioned problems (long period and precision) in simulations and in practice, and to show the effectiveness of using an additional HFS in ISO 9869 [16] Average Method (equivalent to Summation Method in ASTM C1046 and C1155 [17,18]), on the opposite side of the first one, and measuring the heat flux in both sides instead of only one (see Fig. 1). The focus is strictly laid on the usage of the standard method because of its advantage as being the most well-known and applied (due to its simplicity) reference method. Accordingly, in contrast with other aforementioned methods, there is neither the need for a prior knowledge (e.g. transfer functions, grey box modelling, advanced mathematics), nor a new type of equipment (e.g. heater, hotbox). The results of this paper can be easily implemented in ASTM C1046 and C1155 as well.

The further organization of this article includes the research set-up in Section 3, followed by the simulations and their results in Section 4. Later, the experiments and their results are shown in Section 5 and from all results and discussions, conclusions are drawn in Section 6.

## 3. Research set-up and method

The set-up of this research consists of two different phases. At first, finite element simulations are carried out to investigate and demonstrate on different types of walls the difference between the results obtained from the heat flux at each side of the walls. In addition, the results obtained using an average $R_c$-value as defined below and the advantage of reporting this value instead of the two other values ($R_{c-in}$ and $R_{c-out}$) in specific cases values are discussed.

$$R_{c-ave} = (R_{c-in} + R_{c-out})/2 = \left(\sum_{t=0}^{m}\Delta T^t / \sum_{t=0}^{m}\left(\dot{q}^t\right)_1 + \sum_{t=0}^{m}\Delta T^t / \sum_{t=0}^{m}\left(\dot{q}^t\right)_2\right)\Big/2 \tag{4}$$

Secondly, experiments have been carried out to show the benefit of measuring the heat flux at two sides in practice. During the simulations and experiments, the two problems (precision and long monitoring period) are addressed and the benefit of two-sided measurements is illustrated.

## 4. Heat transfer simulations and results

For computational investigation and demonstration, heat transfer simulations have been carried out using COMSOL Multiphysics® 5.3a [38]. This software applies finite element method (FEM) to simulate heat transfer problems. In transient heat transfer, issues such as homogeneity and the position of insulation affects the heat flows significantly [39]. Accordingly, for sake of demonstration, five typologies of walls have been studied: Two homogeneous walls, three insulated walls (insulation placed on the inside, in the middle, and on the outside), and a four-layered cavity wall. The properties and construction of the five types are depicted in Fig. 2 and summarized in Table 1.

The walls' boundary conditions for the simulations include the following:

- Initial Condition: initial temperature 291 K for all solid domains. (average of indoor and outdoor temperature).
- Convective heat transfer coefficient 25 W $m^{-2}$ $K^{-1}$ with outdoor air (lumped convention and IR radiation).
- Convective heat transfer coefficient 7.5 W $m^{-2}$ $K^{-1}$ with indoor air (lumped convection and Infrared radiation).
- Insulation on all lateral sides (1D heat transfer assumption).
- Indoor temperature: winter and summer temperature of 293 K and 296 K (white noise of ±2K amplitude).
- Outdoor temperature: reference Climate Year deBilt 64-65 (one of the typical climate years in the Netherlands).

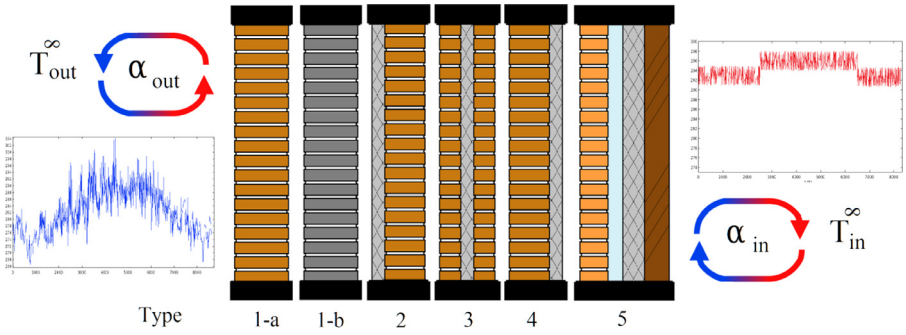


**Fig. 2.** Five typologies modelled in the simulations- All the walls are exposed to forced convection to two air temperature profiles for 8760 h.

**Table 1**
Summary of the five wall types, their dimensions, and their thermal properties.

| Typology | Layer/property | $l$(m) | $k$ [W m$^{-1}$ K$^{-1}$] | $\rho$ [kg m$^{-3}$] | $C$ [J kg$^{-1}$ K$^{-1}$] | $R_c^{th}$ [m$^2$ K W$^{-1}$] |
|---|---|---|---|---|---|---|
| Type 1: Homogeneous | a: Brick | 0.5 | 0.9 | 2000 | 840 | 0.55 |
| | b: Concrete | 0.5 | 1.8 | 2400 | 880 | 0.27 |
| Type 2, 3 and 4: Brick and insulation | Brick | 0.2 | 0.9 | 2000 | 840 | 4.00 |
| | Polyurethane | 0.08 | 0.021 | 35 | 1320 | |
| Type 5: 4-layer cavity wall with insulation and exterior brick facade | Facing brick | 0.10 | 0.900 | 2087 | 87 | 5.31 |
| | Air cavity | 0.04 | $k = k(T)$ | $\rho = \rho(T)$ | $C = C(T)$ | |
| | Polyurethane | 0.10 | 0.021 | 35 | 1320 | |
| | Wood-cement | 0.09 | 0.350 | 1250 | 1470 | |

- Solar radiation, except in 4.4, according to the standard (the use of artificial screening), is not included.
- In 4.4 solar radiation is taken into account in late spring period only to show its negative influence (in other periods of the Dutch climate there is no long-term strong solar radiation to considerably affect the method).
- Rain and snow are neglected as explicitly mentioned in the ISO 9869 [16].

Software settings include time-dependent study, fine, finer, and extra fine mesh, strict hourly time step, and backward differentiation formula time stepping [38]. All simulations have been done for one climate year (hourly temperature data). The calculation of the $R_c$-value from the simulated data has been done for the Dutch heating season (winter, beginning of spring, and end of fall) to assure the reliability of the results. The results presented in Sections 4.1–4.3 belong to winter season (February). As mentioned in the standard, the performance of the method is poor during the summer period and the minimum temperature difference between two sides should be 5 K. Accordingly, this period is not investigated. The duration of the calculation of the cumulative $R_c$-value is up to the time when the test's convergence criteria have been met.

For each typology, the wall is simulated for one year with hourly air temperatures. The indoor and outdoor heat flux is evaluated at two surface cut-points in the middle of each side of the wall, where the HFSs and the thermocouples are supposedly mounted. The output is analysed according to the ISO 9869 [16] Average Method in different periods of the year to check the accuracy and precision. Every 24 h, the two hourly cumulative $R_c$-values (for each side) and their average are reported, using (1). This process continues for a long enough period for a perfect convergence of the three graphs to one actual value (as expected from Table 1), regardless of the mitigation of the ISO 9869 [16] convergence criteria (which happens earlier). Finally, the minimum time required for the ISO 9869 [16] criteria to be met are reported and compared in all cases.

The six modelled walls are categorized as homogeneous and heterogeneous walls. The heterogeneous ones are divided into symmetrical and asymmetrical categories. The results for the $R_c$-value calculation according to (1) are shown for each category. In all figures, solid orange and solid blue are $R_c$-values based on inside ($R_{c\text{-in}}$) and outside ($R_{c\text{-out}}$) heat flux respectively and the dashed black refers to the average $R_c$-value ($R_{c\text{-ave}}$). The arrow gives the point where convergence of $R_c$ is achieved the quickest, according to ISO 9869 criteria.

### 4.1. Homogeneous walls (types 1a and 1b)

The first typology is the homogeneous wall (type 1, see Table 1). For sake of simplicity, minor heterogeneities are neglected (e.g. the mortar joints are considered the same as brick because of their similar thermal properties). The $R_c$-values obtained from two homogeneous walls are plotted in Fig. 3. For the day of convergence and deviation from theoretical value, see Fig. 7.

As seen in both figures, in case of homogeneous walls, the two $R_c$-values converge to the same value, with a similar speed. Mostly, these profiles have a quasi-symmetric shape relative to each other. Therefore, the average of these two will converge quicker to the actual $R_c$-value ($R_c^{th}$). The temperature and heat flux disturbances on each side influence the results on either side whereas the average of the two $R_c$-values shows higher stability. For instance, in the right graph, one would find the $R_c$-value at the 4th day of measurement, using the average $R_c$-value. Using the $R_c$-value based on heat flux on either side, more than 11 days is needed to fulfill the ISO 9869 [16] criteria (see also Fig. 7). In other periods of the year, this duration may be much longer (see Section 4.5).

### 4.2. Heterogeneous walls (types 2, 3, 4, and 5)

Four heterogeneous walls are modelled. The two first models are two-layered walls with one layer of brick and one layer of polyurethane insulation, once at the interior (type 4) and once at the exterior (type 2) side. The third wall is a cavity wall (type 5) and the forth one is similar to the first two, with the insulation in the middle (type 3). The walls are presented in a different order than the number of their types, due to their behavior.

#### 4.2.1. Heterogeneous asymmetrical walls (types 2, 4, and 5)

The two two-layered walls (insulation at inside and outside) and the four-layered cavity wall are presented here as non-

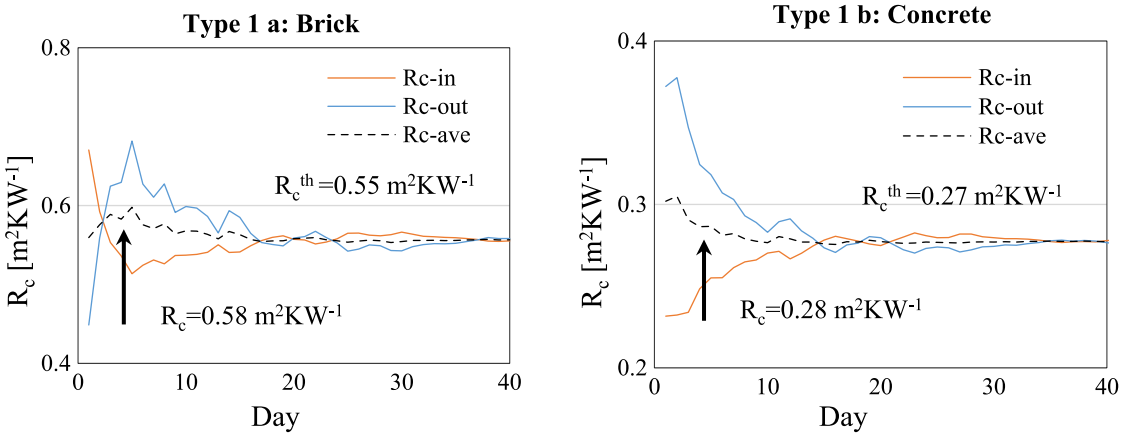


**Fig. 3.** $R_c$-values obtained from each of two homogeneous walls made from brick (left) and concrete (right). The average $R_c$-value converges quicker to the final value.

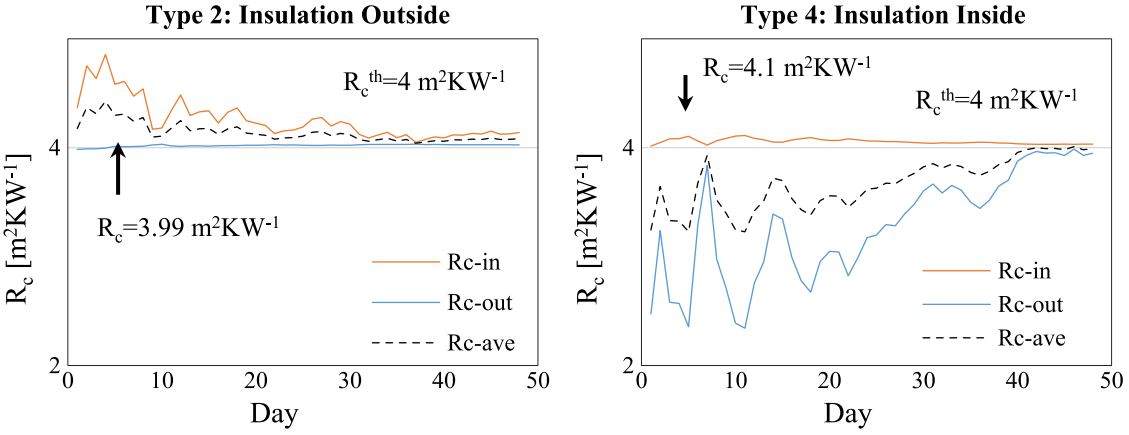


**Fig. 4.** $R_c$-values obtained from each of the types 2 and 4: a homogeneous brick layer with one layer of insulation on the outside (left) and on the inside (right). The $R_c$-value of the side having insulation converges much quicker to the actual value ($R_c^{th}$) in both cases.

homogeneous asymmetrical samples. Although types 2 and 4 are not exactly realistic (in practice, a plaster layer covers the insulation), they are modelled for sake of demonstration of the hypothesis in similar configurations. In Fig. 4, the insulation on the exterior surface, type 2 (left), makes the exterior $R_c$-values graph much more stable and converging very quickly, whereas for the case of type 4, having the insulation on the interior side (right), the one from the interior side is more stable and converges quicker. Using the heat flux at the side closer to the insulation in these two cases results therefore in finding the $R_c$-value in a considerably shorter amount of time. All graphs converge in the end to a value of 4 $m^2$ K $W^{-1}$, as expected from the construction (Table 1).

The result of type 2 (insulation at the outside surface) shows the opposite of what is recommended in ISO 9869, installing the HFS at the side with more stable temperature (indoor). In this case, one would need much longer time to find the $R_c$-value. The reason for this can be referred to the fact that the heat flux at the side with insulation is much more stable than at the side without. As the temperature gradient in two graphs is common, the stability of the heat flux can determine at which side the $R_c$-value graph is more stable, leading to a quicker convergence and therefore earlier estimation of the $R_c$-value. Therefore, in case of only one HFS available, it would be better to place the HFS on the outdoor surface of the wall than on the indoor side. This however, cannot be known in advance and can only be detected by using two HFSs.

The cavity wall is then analysed. This construction belongs to an existing wall in a lab in Leuven, Belgium. In Fig. 5, the result of the $R_c$-value simulations of the cavity wall is presented. The theoretical $R_c$-value is 5.31 $m^2$ K $W^{-1}$ as also reported in [40] (Table 1). The air cavity is modelled with an equivalent thermal conductivity, considering the thermal resistance of the air layer (0.180 $m^2$ K $W^{-1}$ as estimated by [40] and [41]) to include conduction, convection, and IR radiation).

In the modelled cavity wall, similar to type 2 (insulation outside), measuring the HFS at the outer surface of the wall leads to a quicker estimation of the $R_c$-value. This, similar to type 2, in terms of time efficiency, is in contrast with what the ISO 9869 recommends regarding the placement of the sensors at the interior side. This example is underlining again the importance of using two heat flux meters at both sides of the wall for a quicker gain of the $R_c$-value with the same level of accuracy.

*4.2.2. Heterogeneous symmetrical walls (type 3)*

The symmetry is formed by placing the insulation layer in the middle of the wall in between the two brick layers. In Fig. 6, the result for the simulation of the symmetrical heterogeneous wall (type 3) is shown:

As seen in Fig. 6, the interior $R_c$-value converges more quickly than the one from the outdoor. This is due to the fact that the effect of the insulation on the stability of the heat flux is divided between the two surfaces. Therefore, the stability of the temperature plays the dominant role of determining which side results in a quicker and more stable $R_c$-value. Thus, the indoor side $R_c$-value converges more quickly to the actual value of 4 $m^2$ K $W^{-1}$ (Table 1).

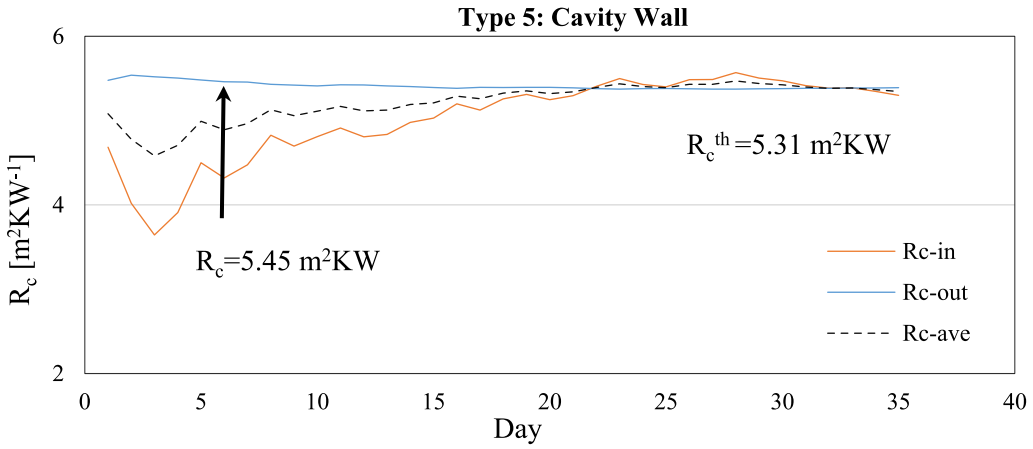


**Fig. 5.** $R_c$-values obtained from type5: 4-layered cavity wall consisting of (from interior to exterior) wood cement, polyurethane, air, and facing brick. The outdoor $R_c$-value has converged much quicker.

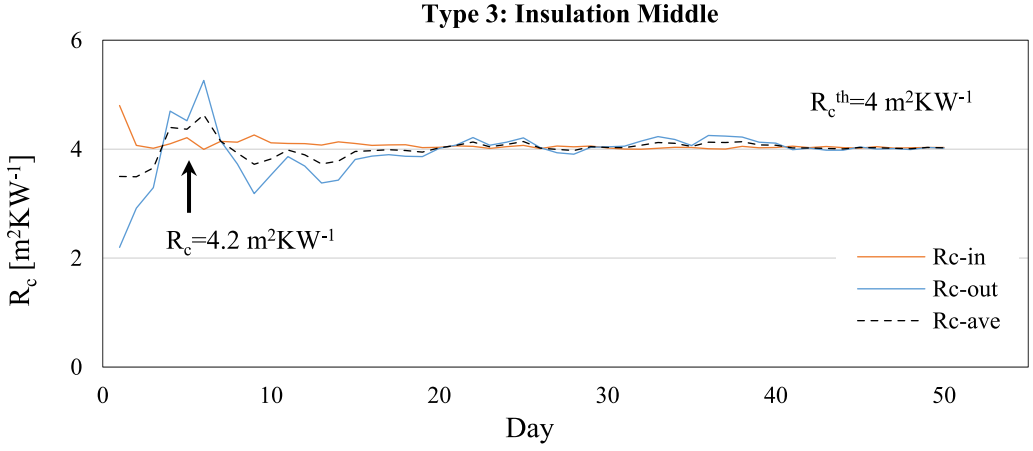


**Fig. 6.** $R_c$-values obtained from the type-3 wall: two homogeneous brick layers connected via insulation in the middle. The effect of the insulation is divided and thus, the side with more stable temperature converges earlier.

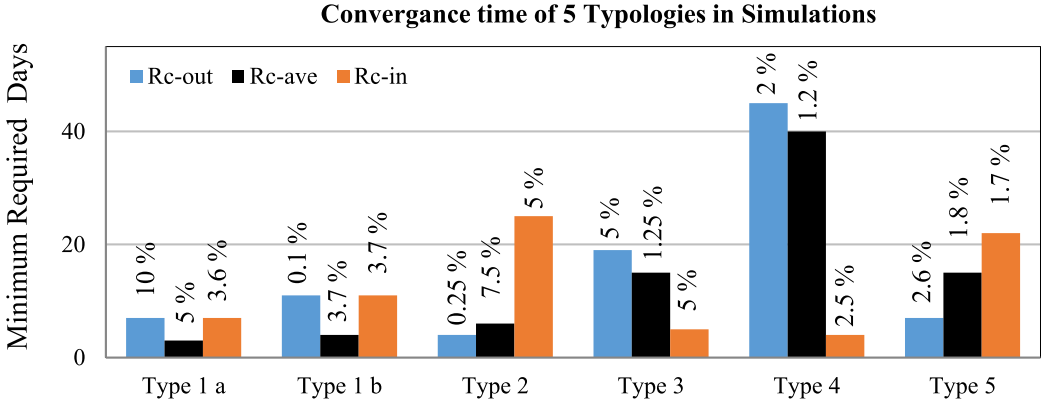


**Fig. 7.** Minimum required time for each typology to fulfill ISO 9869 convergence criteria. The case of which graph converges earlier in case of unknown construction is unpredictable. Inaccuracies are reported in terms of percentage deviation form theoretical value.

### *4.3. Minimum required convergence times*

For sake of comparison, the results of the simulations according to the ISO 9869 [16] criteria are summarized in Fig. 7. The convergence time according to ISO 9869 are assessed and compared and in each case, and the inaccuracy of the measured $R_c$-value (in terms of deviation from the theoretical value) is reported:

As conveyed in Fig. 7, for an unknown construction, it is not possible to predict in advance about which graph will converge earlier to the final value. In types 1a, and 1b, the $R_{c\text{-}ave}$ has converged respectively in half and one-third of the required time (if either of the two heat fluxes were used). In types 2 and 5, $R_{c\text{-}out}$ has converged much more quickly than $R_{c\text{-}in}$ (in less than one sixth of the time in type 2) whereas in types 3 and 4, in agreement with the standard method, the $R_{c\text{-}in}$ has converged much more quickly. However, note that all values reported fulfill the converge criteria of ISO 9869, as described in Section 2.

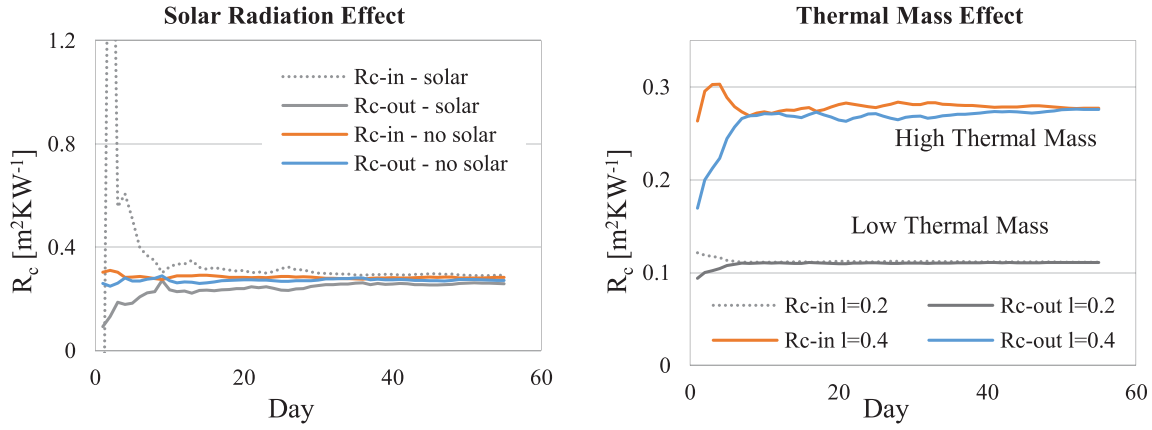


**Fig. 8.** Parameters influencing the convergence of $R_c$-graph. Solar radiation (left) and high thermal mass (right) have negative effects (in grey) while in the absence of these effects, the $R_c$-graphs are more stable and converge earlier.

### 4.4. Parameters influencing the convergence time and stability

Generally, two different aspects affect the stability and convergence of the $R_c$-value graph: the construction (e.g. thermal mass) and the boundary conditions (e.g. solar radiation). In Fig. 8, two examples are shown. The first graph (left) is a concrete wall (type1) exposed to solar radiation (which was excluded in the preceding examples). The presence (in solid and dotted black) and absence (in orange and blue) of solar radiation is shown to compare the stability and convergence of the $R_c$-graph. It is also recommended in the standard to use artificial screening or to exclude the daytime measurements from the results in low thermal mass samples [16]. The second graph (right) shows the effect of thermal mass on the time and quality of the convergence. In case of lower thermal mass ($l$ = 0.2 m), the graph (in solid and dotted black) converges much more quickly and the results are more stable than in case of high thermal mass ($l$ = 0.5 m) (in orange and blue).

### 4.5. $R_c$-value precision problem

The uncertainty of simulations according to ISO 9869 should be around at least 10% (except temperature and heat flow variation error, other errors concern operational, equipment, and calibration error which do not concern simulations). In Fig. 7, all inaccuracies (in terms of deviation from theoretical value) and all precisions (in terms of deviation of the $R_c$-values) were below 10 %. However in certain types of construction, during certain periods of the year, the two $R_c$-values converge, fulfilling the criteria of ISO 9869 (mentioned in Section 2), to two different values which differ by much higher than 10%. This happens most often in homogeneous walls with high thermal mass where stability occurs at the same level on two sides (see Fig. 9). If the extraction of the $R_c$-value continues, the two values take a very long time to reach the same value, the actual $R_c$-value, (see the right part of Fig. 9). This is problematic because both values may be reported while not being within the expected precision range. In such cases, it would be advantageous to use the average $R_c$-value, as it is in the common bandwidth of the two uncertainties and it is closer to the expected value.

In Fig. 9, two cases are shown in which the $R_c$-values have converged to two different values, fulfilling the ISO 9869 criteria at the same time, but differing by more than 10% in precision. These walls (type 1:0.5m brick on the left and 0.5 m concrete on the right) are the same walls shown before, in a different period of time (beginning of fall). The issue has also been occasionally observed in the other types in different periods when temperature and heat flux fluctuations are extreme or when the temperature gradient of the two surfaces becomes small. The arrow gives the point where convergence of $R_c$ is achieved, according to ISO 9869 criteria.

As seen in Fig. 9, the $R_{c\text{-}in}$ and $R_{c\text{-}out}$ graphs converge to different values at the same day, both fulfilling the standard criteria before reaching the final actual value. For the brick wall $R_{c\text{-}in}$ has an inaccuracy of 7.3% and 10% for $R_{c\text{-}out}$. Both values differ by more than 10%. For the concrete wall $R_{c\text{-}in}$ has an inaccuracy of 11% while it is 7.4% for $R_{c\text{-}out}$ which is within an acceptable range. Both values differ by more than 10%. The average of these two graphs in both cases converges much earlier (6th day vs 20th day for the brick wall and 4th day vs 15th day for the concrete wall), with an inaccuracy of less than 4%. Therefore, using the average $R_c$-value is a suitable alternative to waiting for the two graphs to meet at the actual value (far beyond the time to satisfy the convergence criteria of ISO 9869). The occurrence of this problem is not known beforehand, due to the unknown construction and unknown boundary conditions. Therefore, in these cases, it is also of high benefit to measure the heat flux at both sides and if the precision problem is observed, the average value is reported instead of the other two. To even increase the accuracy of the measurement, one can continue the measurement of the average value for a few days more after achievement of the ISO 9869 convergence criteria. This will still be shorter than using the $RC_{\text{-}in}$ value, and more accurate.

## 5. Experimental setup and results

Experiments have been carried out on two case study walls, to show the effectiveness of performing two-sided measurements of heat flux. The first wall is similar to type 3 (insulation inside - the construction is estimated from the appearance). The $R_c$-value is claimed to be 3.5 $m^2$ K $W^{-1}$ according to the value reported in the building permit. The second case is type 1 (homogeneous brick) with the $R_c$-value estimated based on construction (0.21 m wall made of Dutch brick with thermal conductivity of 1.2 W m $K^{-1}$ [42]) as being 0.175 $m^2$ K $W^{-1}$.

Two t-type thermocouples (accuracy 0.5 °C) and two HFP01 HFSs (accuracy 5%) by Hukseflux Thermal Sensors [43] have been mounted on two sides of the wall. The faces of the sensors are covered by paper tape whose emissivity is close to the one from the surface of the wall. Thermal imaging (using FLIR E5 thermal camera) has been employed at first to find the spot which is representative for the whole wall and second, to check if the emissivity's of the sensors' surfaces are the same as the whole wall. This is to avoid different radiation heat transfer, as also recommended by ISO 9869. As explicitly noted in ISO 9869 [16] to protect the exterior surface (e.g. by artificial screening), the exterior surface of the

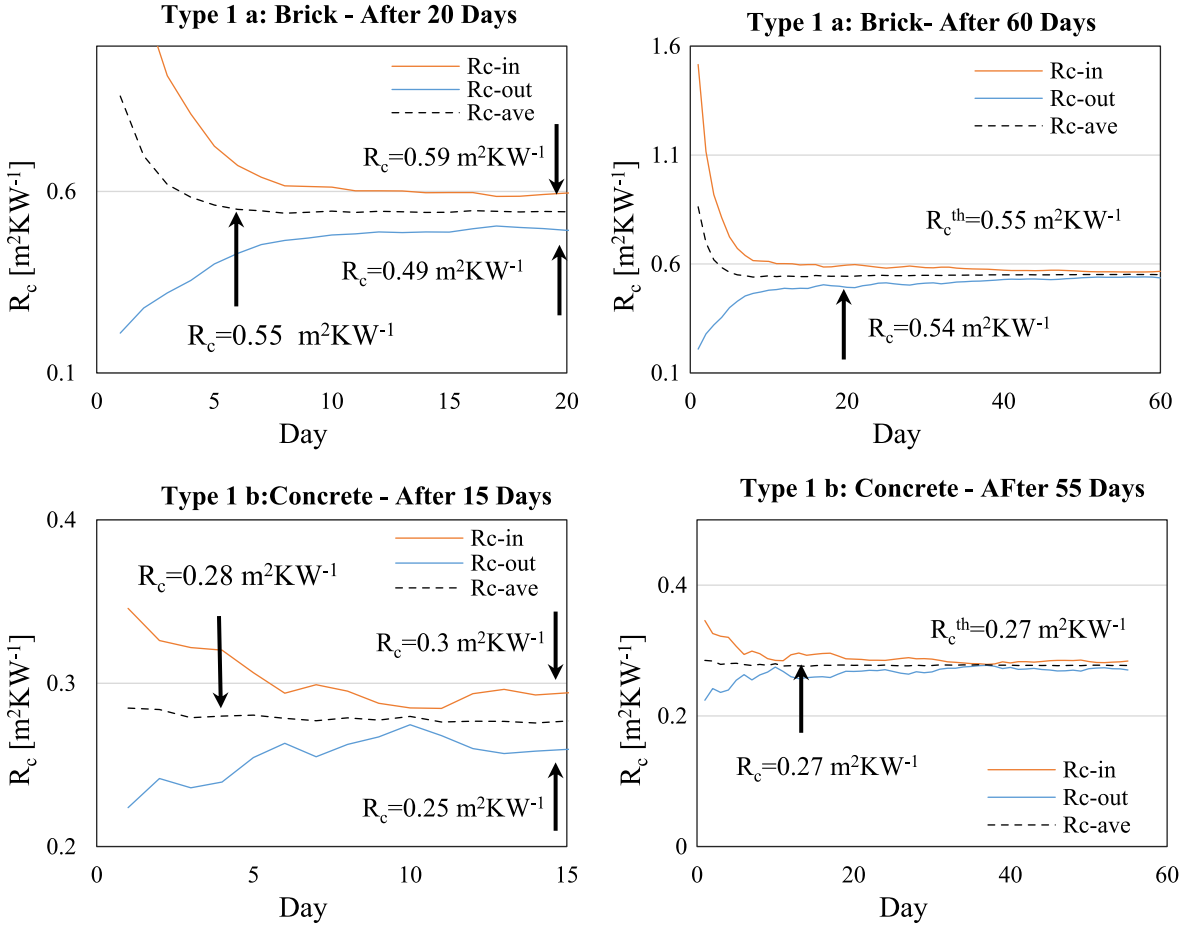


**Fig. 9.** The problem of $R_c$-value precision: two different $R_c$-values (left) are obtained instead of one, both fulfilling the criteria of ISO 9869. The average $R_c$-value is closest to the actual one which the two graphs will converge to, after a very long time (right).

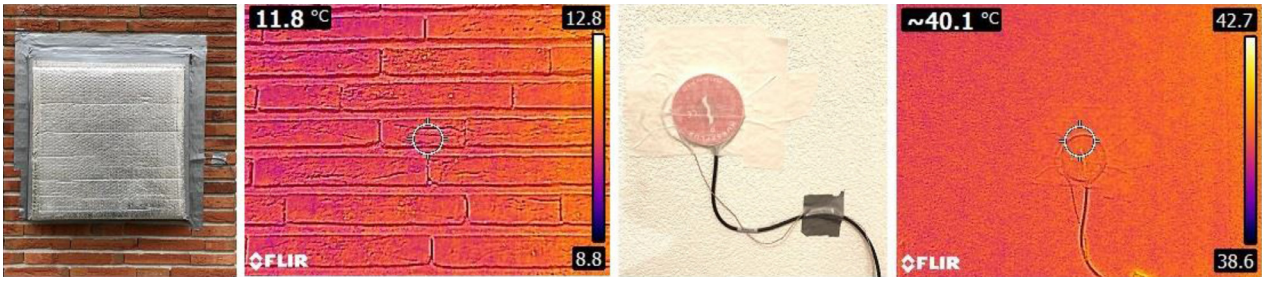


**Fig. 10.** From left to right: the insulation box covering the HFS and the thermocouple outside, the interior side HFS and thermocouple covered with same emissivity tape, IR thermography of the exterior and interior surfaces.

wall is covered with a covering box to minimize the temperature and heat flux perturbations. The box is a square of 60 × 60 $cm^2$ made from Polystyrene and covered with reflective shield to protect the sensors from solar radiation disturbances. The effect of the box has been tested beforehand to ensure limiting the temperature and heat flux noise. The ratio between the area under the box, the area of the sample, and the thickness of the sample is such that the box covers a considerable surface around the sensors while minimizing the 3-D heat transfer effects. In case of high levels of solar radiations and/or larger surfaces, larger protections must be used. Measurements of heat flux and temperature have taken place every second with OMEGA SQ2010 data logger and the hourly averages have been logged. All equipment has been calibrated by the providers before the measurements. In Fig. 10, the experimental setup as well as the IR thermography images are shown.

Measurements have been carried out for long enough periods until the two $R_c$-graphs converge to the same final value. The outcomes of the measurements are presented in the following section.

### 5.1. Case study 1

For the first case study, measurements have been carried out for 16 days. The cumulative $R_c$-value has been calculated by the end of each day using (1), converging to a final value. The results of the $R_c$-value s are plotted in Fig. 11.

Meeting the criteria of ISO 9869, the interior $R_c$-value has converged to 3.55 $m^2$ K $W^{-1}$ at the 5th day with a departure of 1.4% compared to the value reported in the EPC value report by the constructor. According to the criteria of ISO 9869 only the interior $R_c$-value is to be reported. The exterior $R_c$-value seems to need much

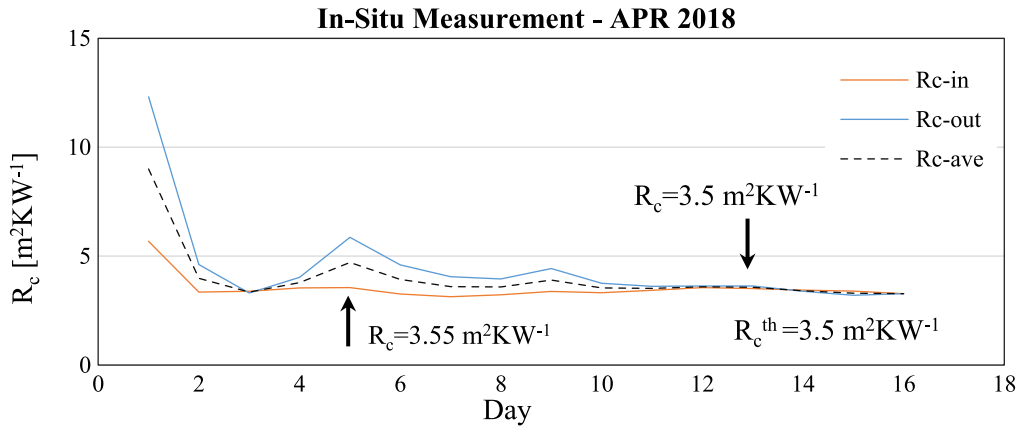


**Fig. 11.** $R_c$-value measurements from case study 1. The indoor heat flux has resulted in the earlier convergence of the $R_c$-value graph. Location: Delft, Netherlands, Apr 2018.

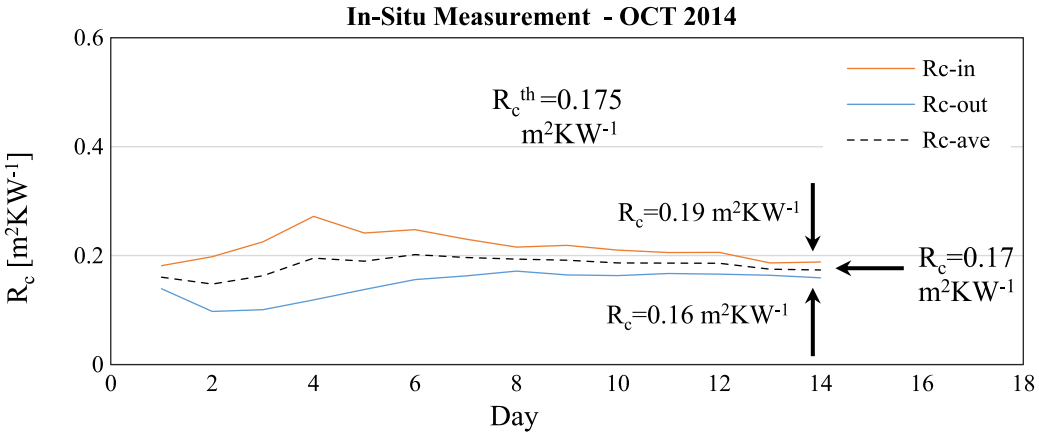


**Fig. 12.** $R_c$-value measurements from case study 2: two different $R_c$-values are obtained, fulfilling the criteria of ISO 9869. Location: The Hague, the Netherlands, Oct 2014.

longer time as it hasn't met the ISO 9869 criteria after 16 days. Despite not meeting the standard criteria, the three graphs have converged to the final value of 3.5 $m^2$ K $W^{-1}$ with an error of within 5%.

### 5.2. Case study 2

During other experiments [44], a case study (case study 2) of a Dutch homogeneous brick wall has been examined. The measurement has been carried out for 14 days and the $R_c$-values have been calculated by the end of each day using (1). The results of the $R_c$-value s are plotted in Fig. 12.

The problem of precision (finding two valid $R_c$-values) has been observed in this case. The two interior and exterior $R_c$-values have converged by a convergence of within 2.5% at the 14th day. The two obtained $R_c$-values are 0.19 $m^2$ K $W^{-1}$ and 0.16 $m^2$ K $W^{-1}$ respectively, leading to an inaccuracy of 8.6% in both cases. The average $R_c$-value however, had converged earlier to 0.17 $m^2KW^{-1}$, which is closest to the theoretical value (inaccuracy of 2.9%).

In such cases, according to what has been shown so far and the mathematics demonstrated, it is recommended to use the average $R_c$-value as it seems to be the most reasonable solution. Especially in this case, because the wall is homogeneous, the average $R_c$-value has converged much better than the other two which will require longer time to meet at the actual value.

## 6. Conclusion

Two problems associated with in-situ measurements based on ISO 9869 [16] have been assessed: duration and precision. The advantage of using two sides' different heat flux time series in $R_c$-value measurements was demonstrated through simulations and measurements. Five typologies of walls have been modelled, showing the advantage of measuring the heat flux at both sides instead of only one. Based on the results of the homogeneous walls, it can be concluded that due to the symmetry of the $R_c$-value graphs, the average $R_c$-value will be closer to the final value and therefore, more reliable than either of the two. Accordingly, the measurement period can be reduced without compromising the accuracy. The average $R_c$-value contributes to solving the problem of $R_c$-value precision as well. In this case, the average $R_c$-value has shown to converge much quicker (up to 10 times quicker) to the actual value. While having the same accuracy, the averaging will avoid finding two different values which are out of 10% precision range.

In case of a heterogeneous wall, the stability of heat flux plays the key role in the convergence of the $R_c$-value graph. The indoor temperature is generally more stable than the outdoor and therefore, ISO 9869 implies placing the HFS in the indoor side. However, as explained in Section 4.2, the effect of heat flux is more critical than the one from temperature. For instance, the effect of outdoor insulation on the stability of the heat flux can become dominant and therefore overcome the negative effect from instability of the outdoor temperature. Accordingly, in case of an insulation layer on exterior side of the wall, or in a cavity wall, it may happen that the outdoor heat flux would result in a much more stable and quicker $R_c$-value whereas the interior heat flux converges much later.

In summary, it is highly recommended that in the in-situ $R_c$-value characterization of unknown constructions, the heat flux would be measured on both sides of the sample rather than only

one. This way, three graphs are generated: $R_c$-values based on inside heat flux, outside heat flux, and the average $R_c$-value. In case one of the $R_{c\text{-in}}$ and $R_{c\text{-out}}$ is more stable and converges earlier than the other, the $R_c$-value from that side should be reported. In case both graphs are instable and symmetrical, mostly happening in homogeneous samples, the average of the two ($R_{c\text{-ave}}$) will converge much quicker and it is the closest to the actual $R_c$-value. This way, the two mentioned problems are tackled. Observing both $R_c$-graphs also provides qualitative information about the possible construction of the wall (e.g. homogeneous, insulation inside, etc.)

The additional costs associated with the suggested modification are generally not high (roughly 5%–20% addition to the total cost). This cost difference (an additional HFS) can be compensated by the fact that by applying the second HFS to the set, the final $R_c$-value can be obtained more quickly, leading to shorter measurement periods. A short measurement period becomes advantageous by allowing more samples to be measured in the same period of time.

## References


[1] L. Belussi, L. Danza, I. Meroni, F. Salamone, Energy performance assessment with empirical methods: application of energy signature, Opto-Electron. Rev. 23 (1) (2015) 85–89.

[2] P. van den Brom, A. Meijer, H. Visscher, Performance gaps in energy consumption: household groups and building characteristics, Build. Res. Inf. 46 (1) (2018) 54–70.

[3] Y. Yang, Innovative Non-Destructive Methodology for Energy Diagnosis of Building Envelope, Bordeaux, 2017.

[4] A. Ioannou, L. Itard, Energy performance and comfort in residential buildings: sensitivity for building parameters and occupancy, Energy Build. 92 (2015) 216–233.

[5] D. Majcen, L. Itard, H. Visscher, Actual and theoretical gas consumption in Dutch dwellings: what causes the differences? Energy Policy 61 (2013) 460–471.

[6] F. Filippidou, N. Nieboer, H. Visscher, Effectiveness of energy renovations: a reassessment based on actual consumption savings, Energy Efficiency (2018) 1–17, doi:10.1007/s12053-018-9634-8.

[7] M.J. Jiménez, H. Madsen, K.K. Andersen, Identification of the main thermal characteristics of building components using MATLAB, Build. Environ. 43 (2) (2008) 170–180.

[8] O. Gutschker, Parameter identification with the software package LORD, Build. Environ. 43 (2) (2008) 163–169.

[9] B. ISO, 6946: 2007 Building Components and Building Elements—Thermal Resistance and Thermal Transmittance—Calculation Method, British Board of Agrément tel, 1923.

[10] P.G. Cesaratto, M. De Carli, A measuring campaign of thermal conductance in situ and possible impacts on net energy demand in buildings, Energy Build. 59 (2013) 29–36.

[11] Baker, P., Technical paper 10: U-values and traditional buildings-In situ measurements and their comparisons to calculated values. 2011.

[12] P. Biddulph, V. Gori, C.A. Elwell, C. Scott, C. Rye, R. Lowe, T. Oreszczyn, Inferring the thermal resistance and effective thermal mass of a wall using frequent temperature and heat flux measurements, Energy Build. 78 (2014) 10–16.

[13] C. Flood, L. Scott, C. Architects, In Situ Thermal Transmittance of Case Studies in Dublin, 2016.

[14] C. Peng, Z. Wu, In situ measuring and evaluating the thermal resistance of building construction, Energy Build. 40 (11) (2008) 2076–2082.

[15] Baker, P., Technical paper 2: in situ U-value measurements in traditional buildings–preliminary results. 2008.

[16] I. ISO, 9869: Thermal Insulation—Building Elements—In-Situ Measurements of Thermal Resistance and Thermal Transmittance, International Organization for Standardization, Geneva, 2014.

[17] C. ASTM, 1046-95 (Reapproved 2001): standard practice for in-situ measurement of heat flux and temperature on building envelope components, in: Annual Book of ASTM Standards, 2001, p. 4.

[18] C. ASTM, 1155-95 (Reapproved 2001): standard practice for determining thermal resistance of building envelope components from the in-situ data, Annual Book of ASTM Standards (2001) 4.

[19] A. Rasooli, L. Itard, C.I. Ferreira, A response factor-based method for the rapid in-situ determination of wall's thermal resistance in existing buildings, Energy Build. 119 (2016) 51–61.

[20] X. Meng, T. Luo, Y. Gao, L. Zhang, Q. Shen, E. Long, A new simple method to measure wall thermal transmittance in situ and its adaptability analysis, Appl. Therm. Eng. 122 (2017) 747–757.

[21] K. Martín, I. Flores, C. Escudero, A. Apaolaza, J.M. Sala, Methodology for the calculation of response factors through experimental tests and validation with simulation, Energy Build. 42 (4) (2010) 461–467.

[22] J.M. Sala, A. Urresti, K. Martín, I. Flores, A. Apaolaza, Static and dynamic thermal characterisation of a hollow brick wall: tests and numerical analysis, Energy Build. 40 (8) (2008) 1513–1520.

[23] B. Yesilata, P. Turgut, A simple dynamic measurement technique for comparing thermal insulation performances of anisotropic building materials, Energy Build. 39 (9) (2007) 1027–1034.

[24] K.N. Agarwal, V.V. Verma, A quick method of measuring thermal conductivity and thermal diffusivity of building fabrics, Build. Sci. 2 (2) (1967) 165–172.

[25] A.J. Robinson, F.J. Lesage, A. Reilly, G. McGranaghan, G. Byrne, R. O'Hegarty, O. Kinnane, A new transient method for determining thermal properties of wall sections, Energy Build. 142 (2017) 139–146.

[26] ISO, B., 8990: 1996, Thermal insulation. Determination of steady-state thermal transmission properties. Calibrated and guarded hot box, BSI, ISBN 0, 1996. 580(26826): p. 8.

[27] G. Baldinelli, A methodology for experimental evaluations of low-e barriers thermal properties: field tests and comparison with theoretical models, Build. Environ. 45 (4) (2010) 1016–1024.

[28] P.G. Cesaratto, M. De Carli, S. Marinetti, Effect of different parameters on the in situ thermal conductance evaluation, Energy Build. 43 (7) (2011) 1792–1801.

[29] F. Wang, D. Wang, X. Wang, J. Yao, A data analysis method for detecting wall thermal resistance considering wind velocity in situ, Energy Build. 42 (10) (2010) 1647–1653.

[30] Deconinck, A.-H. and S. Roels, Comparison of characterisation methods determining the thermal resistance of building components from onsite measurements. Energy Build., 2016. 130: p. 309–320.

[31] A.-H. Deconinck, S. Roels, Is stochastic grey-box modelling suited for physical properties estimation of building components from on-site measurements? J. Build. Phys. 40 (5) (2017) 444–471.

[32] A.-H. Deconinck, S. Roels, The as-built thermal quality of building components: characterising non-stationary phenomena through inverse modelling, Energy Procedia 132 (2017) 351–356.

[33] V. Gori, V. Marincioni, P. Biddulph, C.A. Elwell, Inferring the thermal resistance and effective thermal mass distribution of a wall from in situ measurements to characterise heat transfer at both the interior and exterior surfaces, Energy Build. 135 (2017) 398–409.

[34] A. Ahmad, M. Maslehuddin, L.M. Al-Hadhrami, In situ measurement of thermal transmittance and thermal resistance of hollow reinforced precast concrete walls, Energy Build. 84 (2014) 132–141.

[35] I.A. Atsonios, I.D. Mandilaras, D.A. Kontogeorgos, M.A. Founti, A comparative assessment of the standardized methods for the in-situ measurement of the thermal resistance of building walls, Energy Build. 154 (2017) 198–206.

[36] G. Desogus, S. Mura, R. Ricciu, Comparing different approaches to in situ measurement of building components thermal resistance, Energy Build. 43 (10) (2011) 2613–2620.

[37] K. Gaspar, M. Casals, M. Gangolells, A comparison of standardized calculation methods for in situ measurements of façades U-value, Energy Build. 130 (2016) 592–599.

[38] COMSOL Multiphysics® v. 5.2. www.comsol.com. COMSOL AB, S., Sweden.

[39] D.M.S. Al-Homoud, Performance characteristics and practical applications of common building thermal insulation materials, Build. Environ. 40 (3) (2005) 353–366.

[40] A.-H. Deconinck, Reliable Thermal Resistance Estimation of Building Components from On-Site Measurements, KU Leuven, Belgium, 2017.

[41] B. Kersten, J. van Schijndel, modeling the heat exchange in cavities of building constructions using COMSOL multiphysics®, in: Excerpt from the Proceedings of the 2013 COMSOL Conference in Rotterdam, Rotterdam, Netherlands, 2013.

[42] ISSO, 60, U en R-waarden van bouwkundige constructies, ISSO publicatie, 2005.

[43] Hukseflux Thermal Sensors BV, w.h.c., Delft, The Netherlands.

[44] A. Rasooli, L. Itard, C.I. Ferreira, Rapid, transient, in-situ determination of wall's thermal transmittance, REHVA Eur. HVAC J. 53 (2016) 16–20.